Analyst

ROYAL SOCIETY OF CHEMISTRY

COMMUNICATION

View Article Online
View Journal

Cite this: DOI: 10.1039/d0an00044b

Received 8th January 2020,
Accepted 26th January 2020

DOI: 10.1039/d0an00044b

rsc.li/analyst

Ratiometric fluorescence method for ctDNA analysis based on the construction of a DNA four-way junction†

Guangxing Liu,[a,b] Xiaoyi Ma,[a,c] Yuguo Tang[a,b] and Peng Miao *[a,b]

We present a novel ratiometric fluorescent biosensor for ctDNA analysis based on the construction of a DNA four-way junction (FWJ). Three fuel strands for the FWJ are firstly designed and prepared. Another essential strand for the formation of the structure is the DNA product generated from target ctDNA initiated strand displacement amplification. With the transformation of the DNA structure, the FRET states of two fluorophores change and the ratiometric fluorescence response can be recorded to indicate the level of the initial ctDNA. The proposed method also has excellent capability to discriminate mismatches and shows potential practical utility for clinical samples.

Cancer is one of the leading causes of death worldwide.[1] Thus, early diagnosis and real-time monitoring of cancer have attracted much attention.[2] Tissue biopsy has long been regarded as an important approach.[3] Nevertheless, it suffers from many drawbacks including notorious pain, high cost, easy infection and so on. Liquid biopsy is a minimally invasive method to determine cancer biomarkers with low cost, which only requires blood samples and is patient-friendly.[4] It shows good prospects for efficient diagnosis and prognosis of cancers.[5] Circulating tumor DNA (ctDNA) is a type of extracellular DNA (single-stranded or double-stranded DNA), which is distributed in the peripheral blood and shows high correlations with cancers.[6] Thus, it is considered as one of the most important biomarkers for liquid biopsy and has gradually evolved from basic research to clinical applications.[7] So far, different techniques already exist for the development of novel ctDNA detection methods including the traditional polymerase chain reaction (PCR),[8] surface-enhanced Raman spectroscopy,[9] electrochemical assay,[10] localized surface plasmon resonance,[11] and sequencing.[12] However, these studies are mainly in the early research stages and there are a lot of spaces for further development and optimization. More sensitive and reliable approaches with easy operation and low consumption are still a challenge.

DNA nanotechnology started from Ned Seeman's pioneering work on immobile DNA junctions and folding of DNA into artificial structures. Since then, the development of various DNA nanostructures for theranostic applications has attracted great attention. Inspired by the natural Holliday junction, which is the transient branched DNA intermediate observed in DNA replication,[13] stable three-, four- or more-arm branched junctions can be prepared with appropriate design, hybridization and annealing processes.[14] The formation of these stable junctions can be further applied for biosensing, bioimaging and cargo delivery applications.[15–17] For example, Zou *et al.* integrated DNAzyme into the DNA three-way junction (TWJ) and developed a sensitive fluorescence method for the detection of transcription factors.[18] Huang *et al.* constructed a number of DNA TWJs on the electrode for the recruitment of electrochemical signals by the application of exonuclease III-assisted recycling amplification.[19] Chen *et al.* achieved *in situ* growth of the DNA TWJ on an electrode surface for ultrasensitive detection of target ctDNA.[20] Chumbimuni-Torres's group developed an electrochemical biosensor to determine isothermally amplified Zika Virus RNA by constructing a four-way junction (FWJ).[21]

Fluorescence techniques have been demonstrated to be a powerful research tool.[22,23] Fluorescent biosensors have gained much popularity over other counterparts due to their advantages of high sensitivity, excellent tunability, convenient operation and so on.[24–27] In addition, ratiometric sensing strategies possess self-referencing capability; thus more accurate signals can be obtained. In this contribution, we have developed a ratiometric fluorescence method for ctDNA analysis by the construction of a highly stable FWJ. Strand displacement polymerization is also integrated for signal amplification. After

[a]*CAS Key Lab of Bio-Medical Diagnostics, Suzhou Institute of Biomedical Engineering and Technology, Chinese Academy of Sciences, China. E-mail: miaopeng@sibet.ac.cn ; Fax: +86-512-69588283*

[b]*University of Science and Technology of China, Hefei 230026, China*

[c]*Jinan Guokeyigong Science and Technology Development Co., Ltd, Jinan 250103, China*

†Electronic supplementary information (ESI) available: Fig. S1, 2 and Table S1. See DOI: 10.1039/d0an00044b

optimizing the amplification and detection steps, the sensitivity, selectivity and practical utility have been confirmed. The results indicate that this method is quite promising for the detection of ctDNA and the design may inspire further development of DNA junction based biosensors.

The working principle of the proposed biosensor is illustrated in Scheme 1. Generally, three hairpin-structured DNA probes (FWJ1, FWJ2 and FWJ3) are designed, which remain stable after being mixed together. FWJ1 is labeled with Cy5 at the 5′ end, which emits red fluorescence. FWJ2 is labeled with the fluorescence quencher (Dabcyl) at the 3′ end. In addition, FWJ3 is labeled with FAM and Dabcyl at the 5′ and 3′ ends, respectively. With the rigid hairpin structure, the fluorescence of FAM is effectively quenched on the basis of the FRET mechanism.[28] Therefore, the mixture of the three DNA probes shows strong red emission and nearly no green emission. On the other hand, target ctDNA hybridizes with template DNA, which can be extended by the polymerase. Since the formed double-stranded DNA contains the restriction site of the nicking endonuclease (NEase), a nick is generated and the strand polymerization reaction continues. As a result, a number of FWJ4 strands are released. FWJ4 acts as the bridge DNA and is critical to the formation of the DNA four-way junction, coupling FWJ1, FWJ2 and FWJ3. The structure transition then separates FAM/Dabcyl (FWJ3) and brings Cy5/Dabcyl (FWJ1/2) closer. Therefore, green emission is significantly enhanced while red emission is decreased. By comparing the ratiometric fluorescence signals, highly sensitive detection of ctDNA is achieved.

To check the feasibility of this method, strand displacement amplification and the formation of the four-way junction have been verified by polyacrylamide gel electrophoresis (Fig. S1†). Lane A and B represent the bands of ctDNA and the template for strand displacement amplification (SDA), respectively. In the absence of the primer of ctDNA, polymerization does not occur, and only the template band is observed in lane C. However, after the addition of ctDNA, polymerization and nicking reactions take place. Various bands with different molecular weights are ascribed to the products of polymerization and displacement reactions. On the other hand, in the absence of FWJ4, the three strands of FWJ1, FWJ2 and FWJ3 cannot undergo the self-assembly process, which is evidenced by the band of a relatively low molecular weight. However, after the introduction of FWJ4, a new band with a much higher molecular weight appears, which demonstrates the formation of the four-way junction.

The fluorescence properties of this system are then investigated. As shown in Fig. 1, in the absence of target ctDNA, due to the hairpin structure of FWJ3, the fluorescence of FAM is successfully quenched and strong emission of Cy5 is observed (dashed curves). However, after ctDNA initiated SDA, a number of FWJ4 strands are produced which aid the formation of the four-way junction. As a result, the fluorescence of FAM is significantly enhanced while the fluorescence of Cy5 is decreased (solid curves). The variation of the two fluorescence signals can be used to indicate the presence of target ctDNA.

To achieve optimal sensing performance, certain experimental parameters including DNA concentration, enzyme concentrations, reaction time and incubation temperature are investigated by evaluating the ratios of fluorescence peaks (F_{FAM}/F_{Cy5}). The ratio of Nb.BbvCI and Klenow fragment polymerase is fixed at 5 : 1.[29] F_{FAM}/F_{Cy5} tends to be saturated when the concentrations of DNA and Nb.BbvCI reach 500 nM and 0.1 U μL^{-1} respectively, which are then used as the optimized conditions in the following experiments (Fig. S2A and S2B†). In the absence of target ctDNA, the ratio barely changes after a sufficiently long reaction time. However, after the introduction of ctDNA, strand displacement amplification is triggered and

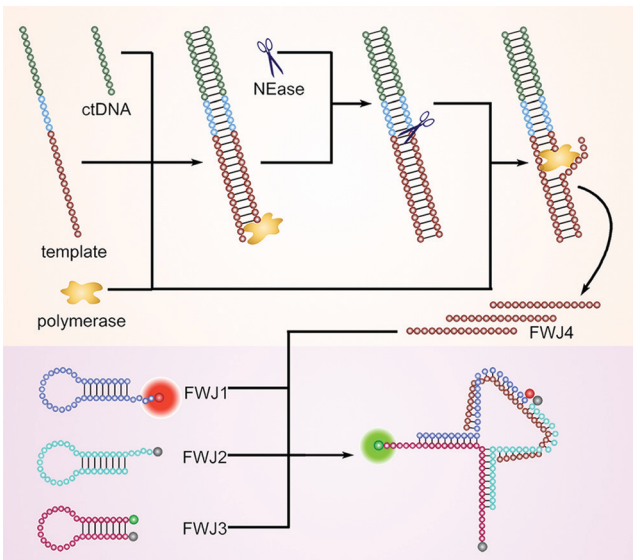

Scheme 1 Illustration of the working mechanism of ctDNA assay.

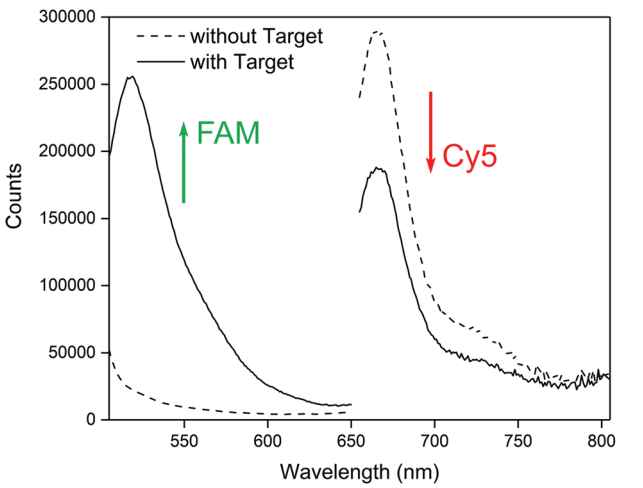

Fig. 1 Fluorescence emission spectra of FAM and Cy5 in the absence and presence of target ctDNA.

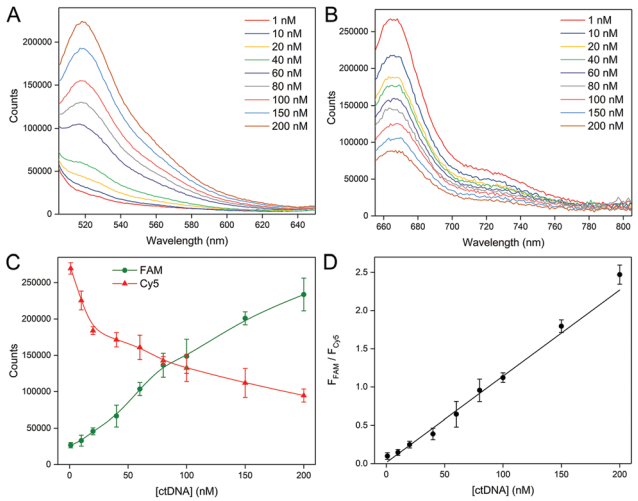

Fig. 2 Fluorescence emission spectra for the detection of ctDNA with concentrations of 1, 10, 20, 40, 60, 80, 100, 150, and 200 nM: (A) FAM; (B) Cy5. (C) The relationship between the ctDNA concentration and the fluorescence intensities of FAM and Cy5. (D) The relationship between the ctDNA concentration and the ratio of the fluorescence intensities.

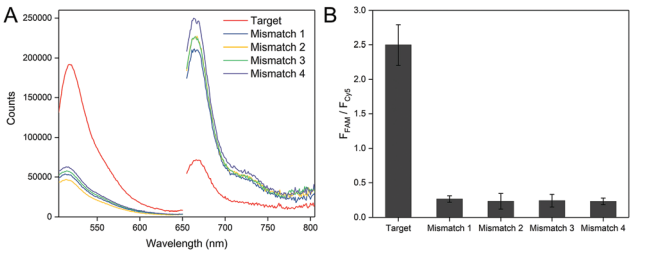

Fig. 3 (A) Fluorescence emission spectra in the presence of target ctDNA and DNA probes with mismatched sites. (B) The fluorescence emission peak intensities.

the four-way junction is formed, leading to changes in the two fluorescence peak intensities. The reaction is nearly completed in 0.5 h, which is reflected by the recorded F_{FAM}/F_{Cy5} (Fig. S2C†). Although the optimal reaction temperature for Klenow fragment polymerase and Nb.BbvCI is 37 °C, higher temperatures may hinder the efficient hybridization of short DNA strands. Therefore, 30 °C is selected for the following experiments, which are more suitable for this fluorescence system (Fig. S2D†).

Under the optimal experimental conditions, the fluorescence spectra of FAM and Cy5 in the presence of a series of concentrations of ctDNA (from 1 to 200 nM) are measured (Fig. 2A and B). It is clear that with a larger amount of ctDNA, the fluorescence of FAM increases while the fluorescence of Cy5 decreases (Fig. 2C). The relationship between the ratio of the two fluorescence peaks and the concentration of ctDNA is evaluated as shown in Fig. 2D. A linear calibration equation is established as follows:

$$y = 0.0138 + 0.0113x \ (n = 3, R^2 = 0.990)$$

in which y is the ratio of the fluorescence peak intensities of FAM and Cy5 and x is the concentration of ctDNA. The limit of detection is calculated to be 0.12 nM according to the 3σ rule (σ is the standard deviation of the blank solutions), which is quite satisfactory after comparing with recently reported DNA assays (Table 1).

We have evaluated the selectivity of this fluorescence system by introducing four mismatched DNA probes. The fluorescence spectra are recorded and compared as shown in Fig. 3, from which it is concluded that the fluorescence responses of the cases of all mismatched DNA probes barely change and the ratio of the fluorescence peak intensities can be successfully distinguished from the target case. Therefore, it may have potential practical utility. We have then spiked different amounts of target ctDNA in a complex matrix of serum samples, which have been diluted ten times so as not to affect the hybridization efficiency of DNA. The corresponding ratiometric responses are in good accordance with those under buffered conditions (Fig. 4). The average recovery is 105.0%, indicating that the proposed method is suitable for use in biological samples.

Table 1 Comparison of the analytical performances of this method with previously developed assays

Technique	Strategy	Detection range (M)	LOD (M)	Ref.
DPV	Graphene quantum dot modified pyrolytic graphite electrode	2×10^{-7} to 5×10^{-7}	10^{-7}	30
ECL	Graphene quantum dots and gold nanoparticles	2.5×10^{-8} to 4×10^{-7}	1.3×10^{-8}	31
SWV	Triplex forming oligonucleotides as the recognizing probes	3×10^{-10} to 3×10^{-6}	3×10^{-9}	32
Colorimetry	Ultrathin transition-metal dichalcogenide nanosheet	2×10^{-9} to 2×10^{-8}	1.54×10^{-9}	33
Colorimetry	Pyrrolidinyl peptide nucleic acid-induced AgNP aggregation	2×10^{-8} to 2.5×10^{-6}	1.03×10^{-9}	34
DPV	Graphene quantum dot modified glassy carbon electrode	10^{-8} to 5×10^{-7}	10^{-9}	35
FET	Coplanar electrode array integrated with a microfluidic chip	10^{-9} to 10^{-5}	10^{-9}	36
Amperometry	FWJ	10^{-9} to 7.5×10^{-8}	9.8×10^{-10}	37
Colorimetry	Three way junction	10^{-9} to 2.5×10^{-7}	9.5×10^{-10}	38
Fluorescence	Silver nanoclusters and carbon oxide nanoparticles	10^{-9} to 5×10^{-8}	4×10^{-10}	39
EIS	Layer-by-layer film of chitosan and carbon nanotubes	10^{-9} to 10^{-7}	1.28×10^{-10}	40
Fluorescence	FWJ and SDA	10^{-9} to 2×10^{-7}	1.2×10^{-10}	This work

DPV, differential pulse voltammetry; ECL, electrochemiluminescence; EIS, electrochemical impedance spectroscopy; FET, field effect transistor; SWV, square wave voltammetry.

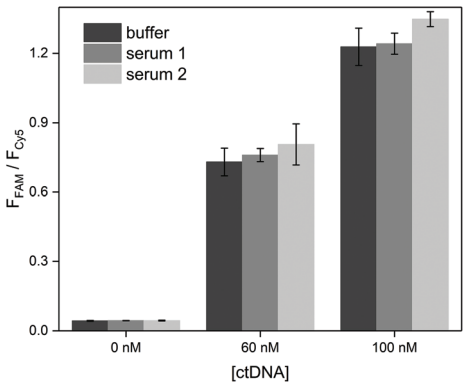

Fig. 4 Fluorescence responses of different concentrations of target ctDNA in buffer and serum (10%) samples.

Conclusions

In summary, a DNA four-way junction based fluorescent biosensor has been well established and optimized for highly sensitive and selective detection of ctDNA. Three hairpin-structured DNA probes remain stable in the system. Only in the presence of the DNA probe produced by the ctDNA initiated SDA reaction, the FWJ is formed and the FRET states of the two fluorophores are changed, whose fluorescence peak intensities vary in the opposite directions. By studying the ratiometric fluorescence response, highly sensitive detection of ctDNA is achieved with a LOD of 0.12 nM. The proposed method also successfully identifies ctDNA in biological samples, which demonstrates its potential for the clinical detection of ctDNA.

Experimental

Materials and chemicals

Sodium chloride (NaCl), sodium dihydrogen phosphate (NaH_2PO_4), sodium hydroxide (NaOH) and dibasic sodium phosphate (Na_2HPO_4) were purchased from Sigma (United States). All DNAs were obtained from Sangon Biotechnology Co. Ltd (Shanghai, China). The sequences are listed in Table S1.† Klenow fragment polymerase, Nb.BbvCI, and dNTPs were purchased from New England Biolabs (Beijing, China). 20 bp DNA Ladder was obtained from Takara Biotechnology Co., Ltd (Dalian, China). Serum samples were collected from Suzhou Science & Technology Town Hospital (Suzhou, China). All other chemicals were of analytical grade and used as received. Double-distilled water was used to prepare all solutions which was purified using a Millipore water purification system with a specific resistance of 18 MΩ cm.

Strand displacement amplification and FWJ formation

All DNA sequences were dissolved in 10 mM phosphate buffered saline (PBS, pH 7.4) with 0.25 M NaCl, and the mixture was heated at 95 °C for 5 min and slowly cooled down to ambient temperature before use. Standard target ctDNA was diluted to a series of concentrations. Subsequently, ctDNA, 0.5 μM template, 250 μM dNTPs, 0.1 U μL^{-1} Nb.BbvCI and 0.02 U μL^{-1} Klenow fragment polymerase were mixed in 10 mM Tris-HCl (50 mM NaCl, 10 mM $MgCl_2$, 100 μg mL^{-1} BSA). The SDA reaction was carried out at 30 °C for 2 h. Afterward, DNA probes including FWJ1, FWJ2 and FWJ3 with a concentration of 0.5 μM were blended with the above mixture for another 0.5 h at room temperature.

Fluorescence measurements

All fluorescence spectra were measured using an FLS1000 Photoluminescence Spectrometer (Edinburgh Instruments, UK). Xenon+ 250 nm grating and Visible PMT R928P were selected as the source light path and detector light path, respectively. Bandwidths for excitation and emission were set at 4 and 3 nm. For FAM measurement, the excitation wavelength was 494 nm and the scan range was from 505 to 650 nm, while for Cy5, the excitation wavelength of 643 nm and the scan range of 655 to 805 nm were applied.

Gel electrophoresis

DNA samples with different treatments and 20 bp Plus DNA ladder were added into the polyacrylamide gel, which were monitored after gel electrophoresis for 50 min (110 V). The gel was stained and photographed under UV light using the Gel Doc XR+ System (Bio-Rad, USA).

Interference investigation and real sample analysis

Four DNA probes with similar sequences with ctDNA were employed instead of the target for the reactions and measurements. After the SDA reaction and junction formation in the presence of these probes (0.5 μM), the fluorescence spectra were measured and compared. To examine the utility of this method in real biological samples, two independent human serum samples were collected and diluted 10 times. Afterward, ctDNA with different concentrations was spiked into these samples. The mixtures were detected by the proposed fluorescence assay.

Conflicts of interest

There are no conflicts to declare.

Acknowledgements

This work is supported by the Science and Technology Cooperation Project between the Chinese and Australian Governments (Grant no. 2017YFE0132300), the Science and Technology Program of Suzhou (Grant no. SYG201909), and the Collaborative Innovation Program of Jinan (Grant no. 2018GXRC033).

Notes and references

1 R. L. Siegel, K. D. Miller and A. Jemal, *CA-Cancer J. Clin.*, 2019, **69**, 7–34.
2 A. Esteva and E. Topol, *Lancet*, 2019, **394**, 1795–1795.
3 D. R. Gandara, S. M. Paul, M. Kowanetz, E. Schleifman, W. Zou, Y. Li, A. Rittmeyer, L. Fehrenbacher, G. Otto, C. Malboeuf, D. S. Lieber, D. Lipson, J. Silterra, L. Amler, T. Riehl, C. A. Cummings, P. S. Hegde, A. Sandler, M. Ballinger, D. Fabrizio, T. Mok and D. S. Shames, *Nat. Med.*, 2018, **24**, 1441–1448.
4 G. Siravegna, S. Marsoni, S. Siena and A. Bardelli, *Nat. Rev. Clin. Oncol.*, 2017, **14**, 531–548.
5 M. Tabata and Y. Miyahara, *J. Mater. Chem. B*, 2019, **7**, 6655–6669.
6 J. Tie, J. D. Cohen, Y. X. Wang, L. Li, M. Christie, K. Simons, H. Elsaleh, S. Kosmider, R. Wong, D. Yip, M. Lee, B. Tran, D. Rangiah, M. Burge, D. Goldstein, M. Singh, I. Skinner, I. Faragher, M. Croxford, C. Bampton, A. Haydon, I. T. Jones, C. S. Karapetis, T. Price, M. J. Schaefer, J. Ptak, L. Dobbyn, N. Silliman, I. Kinde, C. Tomasetti, N. Papadopoulos, K. Kinzler, B. Volgestein and P. Gibbs, *Gut*, 2019, **68**, 663–671.
7 V. Spina, A. Bruscaggin, A. Cuccaro, M. Martini, M. Di Trani, G. Forestieri, M. Manzoni, A. Condoluci, A. Arribas, L. Terzi-Di-Bergamo, S. L. Locatelli, E. Cupelli, L. Ceriani, A. A. Moccia, A. Stathis, L. Nassi, C. Deambrogi, F. Diop, F. Guidetti, A. Cocomazzi, S. Annunziata, V. Rufini, A. Giordano, A. Neri, R. Boldorini, B. Gerber, F. Bertoni, M. Ghielmini, G. Stussi, A. Santoro, F. Cavalli, E. Zucca, L. M. Larocca, G. Gaidano, S. Hohaus, C. Carlo-Stella and D. Rossi, *Blood*, 2018, **131**, 2413–2425.
8 M. B. Freidin, D. V. Freydina, M. Leung, A. M. Fernandez, A. G. Nicholson and E. Lim, *Clin. Chem.*, 2015, **61**, 1299–1304.
9 E. J. H. Wee, Y. L. Wang, S. C. H. Tsao and M. Trau, *Theranostics*, 2016, **6**, 1506–1513.
10 H. F. Wang, R. N. Ma, F. Sun, L. P. Jia, W. Zhang, L. Shang, Q. W. Xue, W. L. Jia and H. S. Wang, *Biosens. Bioelectron.*, 2018, **122**, 224–230.
11 A. H. Nguyen and S. J. Sim, *Biosens. Bioelectron.*, 2015, **67**, 443–449.
12 A. Stahlberg, P. M. Krzyzanowski, J. B. Jackson, M. Egyud, L. Stein and T. E. Godfrey, *Nucleic Acids Res.*, 2016, **44**, e105.
13 Y. Habraken, P. Sung, L. Prakash and S. Prakash, *Nature*, 1994, **371**, 531–534.
14 J. J. Storhoff and C. A. Mirkin, *Chem. Rev.*, 1999, **99**, 1849–1862.
15 D. W. Yang, Y. G. Tang and P. Miao, *TrAC, Trends Anal. Chem.*, 2017, **94**, 1–13.
16 F. M. Shen, H. Qian, Y. L. Cheng, Y. F. Xie, H. Yu, W. R. Yao, R. J. Pei, Y. H. Guo and H. W. Li, *Talanta*, 2020, **206**, 120216.
17 S. Bai, B. Xiu, J. Y. Ye and Y. Dong, *ACS Appl. Mater. Interfaces*, 2015, **7**, 23310–23319.
18 M. Q. Zou, X. Li, D. X. Li, R. Yuan and Y. Xiang, *Sens. Actuators, B*, 2019, **298**, 126865.
19 X. Y. Huang, W. C. Niu, J. Y. Wu, Y. Wang, C. R. Li, J. F. Qiu and J. J. Xue, *Biosens. Bioelectron.*, 2019, **143**, 111609.
20 X. F. Chen, Y. G. Tang, R. H. Yan and P. Miao, *ChemElectroChem*, 2019, **7**, 64–68.
21 C. A. Lynch, M. V. Foguel, A. J. Reed, A. M. Balcarcel, P. Calvo-Marzal, Y. V. Gerasimova and K. Y. Chumbimuni-Torres, *Anal. Chem.*, 2019, **91**, 13458–13464.
22 J. J. Ju, X. F. Peng, K. Q. Huang, L. W. Li, X. H. Liu, C. Chitrakar, L. Q. Chang, Z. P. Gu and T. R. Kuang, *Polymer*, 2019, **180**, 121707.
23 R. L. Sheng, F. F. An, Z. Wang, M. R. Li and A. M. Cao, *RSC Adv.*, 2015, **5**, 12338–12345.
24 Y. Y. Yang, X. F. Wang, G. C. Liao, X. Q. Liu, Q. L. Chen, H. M. Li, L. Lu, P. Zhao and Z. Q. Yu, *J. Colloid Interface Sci.*, 2018, **509**, 515–521.
25 S. J. Sun, Q. W. Guan, Y. Liu, B. Wei, Y. Y. Yang and Z. Q. Yu, *Chin. Chem. Lett.*, 2019, **30**, 1051–1054.
26 C. P. Han, A. W. Zhang, Y. Kong, N. N. Yu, T. Xie, B. R. Dou, K. Li, Y. Wang, J. J. Li and K. Xu, *Anal. Chim. Acta*, 2019, **1067**, 115–128.
27 Y. Yao, D. Zhao, N. Li, F. Z. Shen, J. O. Machuki, D. Z. Yang, J. J. Li, D. Q. Tang, Y. Y. Yu, J. W. Tian, H. F. Dong and F. L. Gao, *Anal. Chem.*, 2019, **91**, 7850–7857.
28 W. Ma, S. N. Sha, P. L. Chen, M. Yu, J. J. Chen, C. B. Huang, B. Yu, Y. Liu, L. H. Liu and Z. Q. Yu, *Adv. Healthcare Mater.*, 2020, **9**, 1901100.
29 X. Y. Ma and P. Miao, *J. Mater. Chem. B*, 2019, **7**, 2608–2612.
30 J. Zhao, G. F. Chen, L. Zhu and G. X. Li, *Electrochem. Commun.*, 2011, **13**, 31–33.
31 Q. Lu, W. Wei, Z. X. Zhou, Z. X. Zhou, Y. J. Zhang and S. Q. Liu, *Analyst*, 2014, **139**, 2404–2410.
32 S. Cinti, E. Proietti, F. Casotto, D. Moscone and F. Arduini, *Anal. Chem.*, 2018, **90**, 13680–13686.
33 L. Y. Lan, Y. Yao, J. F. Ping and Y. B. Ying, *Sens. Actuators, B*, 2019, **290**, 565–572.
34 P. Teengam, W. Siangproh, A. Tuantranont, T. Vilaivan, O. Chailapakul and C. S. Henry, *Anal. Chem.*, 2017, **89**, 5428–5435.
35 Q. Xiang, J. Y. Huang, H. Y. Huang, W. W. Mao and Z. Z. Ye, *RSC Adv.*, 2018, **8**, 1820–1825.
36 H. E. Kim, A. Schuck, J. H. Lee and Y. S. Kim, *Sens. Actuators, B*, 2019, **291**, 96–101.
37 D. M. Mills, M. V. Foguel, C. P. Martin, T. T. Trieu, O. Kamar, P. Calvo-Marzal, D. M. Kolpashchikov and K. Y. Chumbimuni-Torres, *Sens. Actuators, B*, 2019, **293**, 11–15.
38 H. Zhang, X. T. Li, F. He, M. Q. Zhao and L. S. Ling, *Sci. Rep.*, 2018, **8**, 12021.
39 Y. D. Ye, L. Xia, D. D. Xu, X. J. Xing, D. W. Pang and H. W. Tang, *Biosens. Bioelectron.*, 2016, **85**, 837–843.
40 J. C. Soares, A. C. Soares, V. C. Rodrigues, M. E. Melendez, A. C. Santos, E. F. Faria, R. M. Reis, A. L. Carvalho and O. N. Oliveira, *ACS Appl. Mater. Interfaces*, 2019, **11**, 46645–46650.